Assessment of Radial Distortion Parameter Variability in Airborne Photogrammetry: Implications for Atmospheric Refraction

Assessment of Radial Distortion Parameter Variability in Airborne Photogrammetry: Implications for Atmospheric Refraction

Myrta Maria Macelloni [1], Nives Grasso [1], Alberto Cina [1]

[1] Department of Environment, Land and Infrastructure Engineering (DIATI), Politecnico di Torino, Torino (Italy) – (myrta.macelloni, nives.grasso, alberto.cina)@polito.it

Keywords: Glacier monitoring, refraction, photogrammetry, camera calibration

Abstract

The Valpelline Valley, located in the northern Aosta Valley (Italy) along the Swiss border, is a typical Alpine valley shaped by glacial and fluvial processes. Characterized by a large altitudinal range (900-4000 m a.s.l.) and hosting glaciers feeding the Place Moulin reservoir, the area plays a key role in regional hydroelectric production. Since 2020, GlacierLAB has been conducting glacier monitoring activities through biannual aerial photogrammetric surveys, overcoming the logistical constraints imposed by the steep and inaccessible morphology of the valley.

The surveys were performed using a medium-format camera mounted under an aircraft wing and equipped with GNSS and IMU systems. Due to the lack of synchronization between the camera shutter and GNSS receiver, georeferencing relied on Ground Control Points (GCPs), whose spatial distribution is often limited in high-mountain environments. This condition makes camera calibration a critical factor for ensuring reliable multi-temporal analysis.

This study investigates the behavior of the radial distortion parameter k_1 using images previously corrected for optical distortion. A multi-run bundle adjustment strategy was applied in Agisoft Metashape, including baseline configurations, global and image-wise estimation of k_1, and robustness tests under different GCP setups. Statistical analyses reveal a systematic and significant dependence of k_1 on the vertical camera–terrain distance.

However, comparison with a theoretical atmospheric model based on the Saastamoinen formulation shows weak correlation, indicating that the observed effect cannot be attributed solely to atmospheric refraction. Instead, k_1 acts as a compensatory parameter absorbing depth-dependent systematic effects related to block geometry and acquisition conditions.

1. Introduction

Climate change is having a strong impact on mountainous areas, particularly in Alpine regions. In the coming decades, these environments are expected to experience an increase in extreme events, significant environmental changes, and growing impacts on local populations. Glaciers have been rapidly retreating in recent decades, accompanied by a reduction in snow cover, rising temperatures, and permafrost degradation (Beniston et al., 2018; Hugonnet et al., 2021). Glacier mass loss has accelerated, with thinning rates of approximately 1 m per year between 2000 and 2019 and a total ice volume loss of up to 43% since the 1980s (Jacquemart et al., 2024, Zemp et al., 2019). According to IPCC reports (2023), Alpine glaciers could lose up to 94% of their volume under high-emission scenarios.

These changes have significant implications for hydrological regimes, as glacier meltwater currently plays a crucial role in sustaining river discharge, particularly during dry summer periods (Viviroli et al., 2007; Hock et al., 2019). However, once glaciers pass their peak water contribution, a decline in runoff is expected, potentially leading to water shortages for downstream communities, agriculture, and hydropower production (Immerzeel et al., 2010). Moreover, the frequency and intensity of natural hazards are projected to increase in the coming decades. Glacier retreat and permafrost degradation contribute to slope destabilization, resulting in a higher occurrence of rockfalls, debris flows, and glacial lake outburst floods (Stoffel et al., 2014; Haeberli et al., 2017; WSL SLF, 2025).

Within this context of rapid environmental change, accurate monitoring of Alpine areas becomes increasingly important, yet also more challenging. Alpine environments are characterized by very large elevation differences between valley floors and surrounding peaks, as well as by significant difficulties in the materialization of ground control points. These challenges arise both from the time and qualified human resources required and from the limited accessibility of many locations.

Therefore, for environmental monitoring in mountainous areas, the estimation of atmospheric refraction error plays a crucial role, although it remains difficult to model accurately. In photogrammetric processing, the estimation of calibration parameters through least-squares adjustment does not exclusively reflect the physical optical distortion of the camera. Instead, these parameters may absorb multiple sources of error, including measurement inaccuracies, block geometry weaknesses, and the spatial distribution of Ground Control Points. Atmospheric refraction, which is generally negligible in close-range applications, becomes increasingly significant at high altitudes and long acquisition distances, where its effect is proportional to the camera-to-object distance and strongly influenced by acquisition conditions such as oblique imagery. As a result, the estimated parameters are not solely representative of lens distortion but also incorporate additional systematic effects that are difficult to separate. This issue is particularly critical in mountainous environments, where weak GCP (Ground Control Points) configurations and mixed acquisition geometries (nadir and oblique images) are common.

In analogy with geodetic and topographic practices, where systematic errors are modeled separately to ensure physical consistency, it is therefore essential in photogrammetry to distinguish between optical distortion, atmospheric refraction, and random errors related to control point accuracy. Such separation allows for a more reliable interpretation of calibration parameters and improves the robustness of multi-temporal analyses in complex high-mountain environments.

2. Case study

The Valpelline Valley (Figure 1) is the longest valley in the Aosta Valley region, extending from the Great St. Bernard Valley near Gignod up to the Collon Pass, which marks the border with the Swiss Valais. The valley is traversed along its entire length by the Buthier stream, which flows through high-altitude peaks and glaciated areas. The stream originates from the Tsa de Tzan Glacier and the Grandes Murailles Glacier, forming the Place Moulin Lake through an artificial dam before continuing downstream and joining the Dora Baltea River near Aosta.

The Place Moulin reservoir represents one of the most important energy infrastructures in the region, highlighting how the valley's morphology has been effectively exploited for hydroelectric power production. However, the impacts of climate change are not limited to glacier retreat alone. In June 2024, intense high-altitude rainfall triggered the collapse of the lateral moraine of the Tsa de Tzan Glacier, affecting an area of approximately 70000 m². The resulting effects propagated along the Buthier de Valpelline stream in the form of erosion, debris flows, and sediment transport, reaching the intake of the Place Moulin dam with an estimated volume of about 6 million cubic meters of water and debris (Legambiente, 2024).

Glaciers play a fundamental role in regulating water discharge, acting as a crucial freshwater source for both mountainous areas and downstream regions. Their ongoing shrinkage also accelerates sediment release, potentially increasing hydrogeological instability (ISPRA, 2024). Projections indicate a significant reduction in summer water availability, ranging between 15% and 40% as early as 2035, particularly during the peak demand period (Sottozero, 2025).

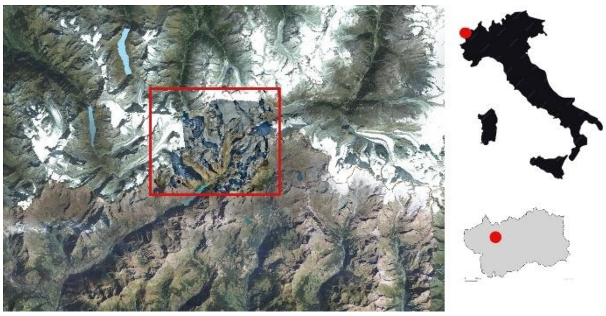

Figure 1. Case study area.

3. Materials and methods

The Valpelline Valley is monitored by the Politecnico di Torino in collaboration with the ARPA Valle d'Aosta, with the support of a Turin-based company, Digisky. Biannual aerial surveys are conducted to systematically cover the entire valley. Main characteristics of the flights are reported in Table 1.

For this purpose, a PhaseOne iXM-RS150F digital camera (151.3 MP, medium format) equipped with 50 mm optics and a sensor size of 40 mm × 53.5 mm is mounted under the wing of the aircraft. The airborne platform is also equipped with a Global Navigation Satellite System (GNSS) antenna and an Inertial Measurement Unit (IMU) with metric accuracy, enabling the acquisition of georeferenced photogrammetric data over the study area. In July 2020, a photogrammetric flight by Digisky company has been made over Valpelline Valley within the activities of the Glacier Lab of the DIATI, Politecnico di Torino. In October 2022, in collaboration with ARPA Valle d'Aosta a second flight with the same camera was carried out in the Valpelline Area. In November 2024, a third flight was executed over the same area and larger. All the flight were centred on the Place Moulin dam and the Buthier river and the steep areas around.

Table 1. Characteristics of the photogrammetric flights.

Flight	Average flight height agl (above ground level) [m]	GSD [m]
July 2020	1000	0.5
October 2022	1000	0.5
November 2024	1000	0.5

Given the high-altitude acquisition conditions and the complex morphology of the study area, a dedicated photogrammetric processing strategy was implemented, with particular attention to camera calibration and the potential influence of atmospheric refraction.

The camera calibration results were analyzed according to the Brown–Conrady distortion model, in which radial distortion is described by the coefficients k_1, k_2, k_3 tangential distortion by p_1, p_2, and affinity and non-orthogonality by additional parameters such as B_1 and B_2. In this framework, the image coordinate corrections can be expressed as:

$$\delta x = x\,(k_1 r^2 + k_2 r^4 + k3\, r^6) + 2p_1 xy + p_2 (r^2+2x^2) + B_1 x + B_2 y$$
$$\delta y = y\,(k_1 r^2 + k_2 r^4 + k_3 r^6) + 2p_2 xy + p_1 (r^2+2y^2) \quad (1)$$

where $r^2=x^2+y^2$. Although the Brown model can include up to 11 parameters, not all of them contribute equally to the description of optical distortion. The analysis of the correlation matrix obtained from the calibration of the PhaseOne 151 MP camera (50 mm focal length as already wrote) highlights that the parameters B_1, B_2, k_1, k_2, k_3 are associated with the largest eigenvalues, thus representing the dominant components of the model. Conversely, higher-order radial terms (k_4) and tangential components (p_1, p_2) exhibit low variance and can be considered negligible in this specific case.

This result confirms that the use of an over-parameterized model may lead to instability in the estimation process, particularly in the presence of limited or unevenly distributed GCPs. In such conditions, calibration parameters do not exclusively represent physical lens distortion but may also absorb other sources of systematic error. In particular, the first radial distortion coefficient k_1 , which typically captures the dominant radial component of optical distortion, can act as a compensatory term within the bundle adjustment.

In high-altitude photogrammetric surveys, such as those performed in Alpine environments, atmospheric refraction introduces additional systematic effects that are proportional to the camera-to-object distance and influenced by acquisition geometry. These effects cannot be explicitly modeled within the standard Brown formulation and may therefore be partially absorbed by the estimated distortion parameters, especially k_1. As a consequence, the interpretation of k_1 as a purely optical parameter becomes ambiguous, as it may include contributions from residual geometric errors, GCP configuration weaknesses, and atmospheric effects.

This highlights the importance of adopting a parsimonious calibration model and of interpreting estimated parameters within the broader context of acquisition geometry and environmental conditions. In particular, separating optical distortion from atmospheric refraction, similarly to the decomposition of systematic errors in geodetic models, is essential to ensure a physically meaningful interpretation of calibration results (Brown, 1971; Fraser, 1997; Remondino and Fraser, 2006).

3.1 Measurements Campaigns and control points

Different measurement campaigns were conducted between 2020 and 2022 to materialize and survey a set of points along the valley, from the Place Moulin dam up to the Capanna Aosta hut. In 2024, an additional campaign was carried out to increase the spatial distribution of points, focusing on the measurement of natural features (e.g., clearly identifiable terrain points, rock edges, and bivouacs), which were surveyed by helicopter.
These campaigns aimed to collect reference points within the study area using GNSS (Global Navigation Satellite System) in RTK (Real-Time Kinematic) mode, achieving centimetric accuracy.

3.2 Data processing

The acquired images were oriented and processed as a photogrammetric block using Agisoft Metashape Professional (version 2.2.1), based on the points measured during the field campaigns. The processing workflow followed a standard Structure-from-Motion (SfM) approach, including image alignment, camera orientation, and sparse point cloud generation. The measured points were used as GCPs to georeference the model and improve its overall accuracy, enabling a more robust estimation of the exterior orientation parameters and reducing potential systematic errors. Subsequently, a dense point cloud was generated, followed by the derivation of a digital surface model (DSM) and orthophoto.
In order to investigate the effect of atmospheric refraction, a second processing workflow was implemented. The same set of images was first corrected for lens distortion using the calibration certificate of the PhaseOne camera through a dedicated MATLAB script. This correction removed lens-induced geometric deformations, ensuring that the image geometry approximates an ideal pinhole camera model. Performing this step prior to photogrammetric processing minimizes systematic errors related to radial and tangential distortions and improves the reliability of camera orientation and 3D reconstruction. Moreover, applying the undistortion in a controlled environment ensured consistency across datasets and acquisition campaigns.
The aim of the analysis is to assess whether, starting from aerial images previously undistorted using known internal calibration parameters, the radial distortion parameter k_1 re-estimated during the bundle adjustment exhibits a systematic dependence on the vertical distance between the camera center and the terrain surface. Such dependence is interpreted as a potential indicator of residual effects related to block geometry or to physical phenomena, including atmospheric refraction.
The refraction analysis was then carried out in Metashape using the undistorted images. Camera intrinsics were initialized according to a pinhole model, with focal length, pixel size, and principal point fixed, while all distortion coefficients (k_1 to k_4, p_1, p_2, B_1, B_2) were set to zero. A multi-run bundle adjustment strategy was adopted to evaluate the role of residual radial distortion.
Four processing configurations were tested.

- In the first run, all intrinsic parameters were fixed, providing a baseline solution (Run1).
- In the second run, only the first radial distortion coefficient (k_1) was estimated at the camera group level, while all other parameters remained fixed (Run2).
- In the third run, k_1 was estimated independently for each image in order to assess its variability with respect to the acquisition geometry (Run3).
- Finally, robustness tests were carried out by modifying the GCP configuration, including partial removal and reclassification of selected GCPs as check points (Run4a and Run4b). For each configuration, the bundle adjustment outputs were analyzed in terms of reprojection error, RMSE on GCPs and check points, and estimated intrinsic parameters.

For each configuration, bundle adjustment outputs were evaluated in terms of reprojection error, RMSE on GCPs and check points, and estimated intrinsic parameters. For each image iii, the vertical distance between the camera center and the observed terrain was computed as

$$dZ_i = Z_{cam,i} - Z_{terrain,I} \tag{2}$$

The relationship between the estimated parameter $k_{1,i}$ and dZ_i was investigated through a set of complementary statistical analyses.
Fist, the linear regression (Ordinary Least Square, OLS) was computed according to the formula:

$$K_{1,i} = \beta_0 + \beta_1\, dZ_i + \varepsilon_i \tag{3}$$

where $K_{1.i}$ value K_1 for each image i, dZ_i is the vertical distance between the camera and the terrain, β_0 represents the intercept, while β_1 represents the slope of the regression model and ε_i the residual error.
To verify that the observed relationship was not driven by outliers, a robust regression model was also applied.
Finally, the multiple regression was estimated according to the formula:

$$K_{1,i} = \beta_0 + \beta_1\, dZ_i + \beta_2\, n\_marker\_obs_i + \varepsilon_i \tag{4}$$

Where β0 is the intercept, β1 is the slope associated with the vertical distance dZi, β2 is the coefficient related to the number of observed markers $n\_marker\_obs_i$ (used as an indicator of local geometric robustness, ε_i is the residual error term.
From a physical perspective, atmospheric refraction was considered as a systematic effect related to variations in the refractive index of air along the optical path. Atmospheric refraction is an angular distortion Δα of the optical ray that strikes the camera sensor at a point located at a distance r′ from the principal point, instead of r. The equation is:

$$\Delta\alpha = K \tan \alpha_i \tag{5}$$

Where α is the angle with respect to the vertical, Δα is the deviation angle from the straight path and K=dn/n is the relative variation of the atmospheric refractive index.
Let f be the principal distance of the camera, r′ the distance between the principal point and the correct position of the image point, and r the true distance:

$$r = r' + \Delta r$$
$$r' = r - \Delta r = f \tan(\alpha - \Delta\alpha) \tag{6}$$

Developing the equation we obtain:

$$\Delta r = -K\,(r + r^3 / f^2) \tag{7}$$
$$\Delta x = (x/r)\,\Delta r = -K\,(1 + r^2 / f^2)\,x$$
$$\Delta y = (y/r)\,\Delta r = -K\,(1 + r^2 / f^2)\,y$$

We compare (7) with the corrections for radial optical distortions (coefficients *k*), tangential (coefficients *p*) according to the Brown model (1). Considering only parameter k_1 and setting the others to zero we obtain:

$$\delta x = k1\, r^2\, x \tag{8}$$
$$\delta y = k1\, r^2\, y$$

which are equivalent to the second term of (7) assuming $K = -k_1 f^2$.
To quantify the effect of atmospheric refraction at different

terrain elevations h and flight altitudes H (expressed in km), the formulation proposed by Saastamoinen (1974) was applied, as it provides a practical approximation depending only on these variables.

$$K=[13(H-h)\,[1-0.02(2H+h)]]10^{-6} \quad (9)$$

This formulation provides an estimate of the expected signal magnitude and supports the interpretation of the residual systematic effects observed in the bundle adjustment, although it does not explicitly model the ray bending within the photogrammetric framework. The expression can also be reformulated in polynomial form:

$$aH^2+bH+ch^2+dh+ehH-K=0 \quad (10)$$

where the coefficients a,b,c,d, and e are estimated through a least-squares adjustment.
The parameter estimation was performed starting from the values of k_1 obtained for each image through bundle adjustment in Agisoft Metashape, using a photogrammetric block composed of 215 previously undistorted images.

4. Results

Cartographic products, such as Digital Surface Models (DSMs) and orthophotos, were derived from the different photogrammetric solutions. While the processing was initially carried out for general mapping purposes, the resulting m odels were further exploited for the analysis of calibration parameter behavior.
First, the RMSE values obtained from the different runs were compared with those of the original non-undistorted block, in order to assess the effect of image undistortion and control point configuration. The comparison was carried out considering both a GCP-only solution and a configuration including GCPs and check points consistent with run 4b (Table 2).

Table 2. RMSE comparison of the different runs and the original (distorted) block under different control point configurations

Run Name	n. GCP	n. CP	RMSE			
			GCP xy [m]	GCP z [m]	CP xy [m]	CP z [m]
Run1	19	-	0.031	0.010	-	-
Run2	19	-	0.018	0.003	-	-
Run3	19	-	0.025	0.008	-	-
Run4a	9	10	0.023	0.010	0.282	0.462
Run4 b	8	11	0.025	0.008	0.305	0.573
Ori GCP	19	-	0.078	0.088	-	-
Ori GCP &CP	8	11	0.046	0.136	0.191	0.364

Within the described framework, runs 1 and 2 are used only as baseline configurations and are not included in the physical interpretation, as the parameter k_1 remains constant across the block, making it unsuitable for evaluating its dependence on the camera–terrain distance.
The analysis therefore focuses on Run 3, in which k_1 is estimated independently for each image, allowing a direct comparison with the vertical camera–terrain distance (dZ). The OLS regression highlights a positive and statistically significant relationship between k_1 and dZ.

The OLS regression highlights a positive and statistically significant relationship between k_1 and dZ (Table 3).

Table 3. Linear and robust regression results between K1 and camera-to-terrain distance (dZ) for runs 3, 4a and 4b.

Run	Slope (OLS)	Slope (robust)	r	R^2	p-value
Run3	7.14×10^{-7}	6.10×10^{-7}	0.606	0.368	5.63×10^{-23}
Run4a	7.60×10^{-7}	6.97×10^{-7}	0.638	0.407	5.46×10^{-26}
Run4b	6.96×10^{-7}	6.30×10^{-7}	0.595	0.354	6.06×10^{-22}

The robustness of this relationship was evaluated through Runs 4a and 4b, characterized by different GCP/check point configurations. The results show that regression slopes remain consistent across runs, while both OLS and robust estimates are stable and the distributions of k_1 are comparable (Table 3, Figure 2 and Figure 3).

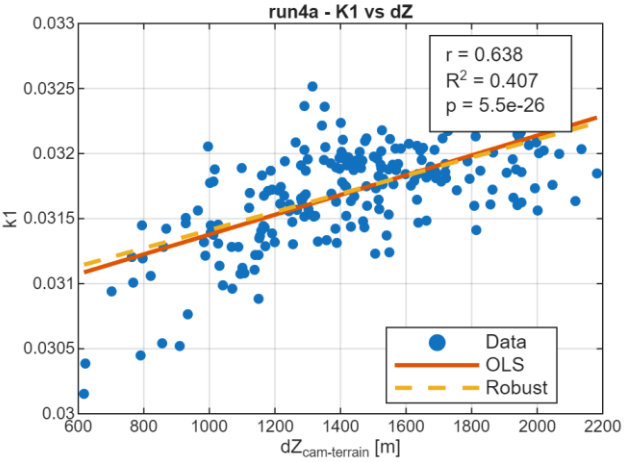

Figure 2. Relationship between K1 and camera-to-terrain distance (dZ) for Run 4a.

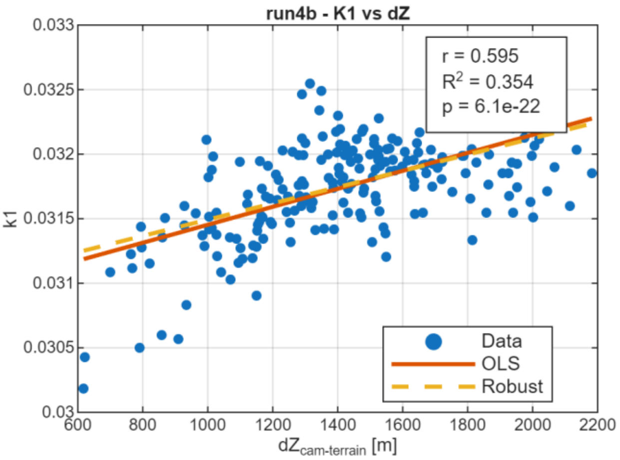

Figure 3. Relationship between K_1 and camera-to-terrain distance (dZ) for Run 4b.

This demonstrates that the observed relationship is independent of the control point configuration and therefore represents a stable characteristic of the photogrammetric block rather than an artifact of the network design.
To further assess the influence of local geometric conditions, the number of observed markers per image was analyzed as a function of dZ. The results (Table 4) show an increasing trend of

marker observations with increasing dZ, indicating that images acquired at greater distances are not less constrained. Consequently, the observed relationship between k1 and dZ cannot be attributed to weaker local geometry.

Table 4. Multiple regression results for K1 as a function of dZ and the number of observed markers.

Run	β_dZ	p_dZ	β_nMarker	p_nMarker	R^2
Run 3	7.81×10^{-7}	6.36×10^{-20}	-2.77×10^{-5}	0.118	0.375

This finding excludes a simple explanation based on reduced photogrammetric robustness at larger distances.
The relationship between the estimated parameter and the camera-to-terrain distance is shown in Figure 4.

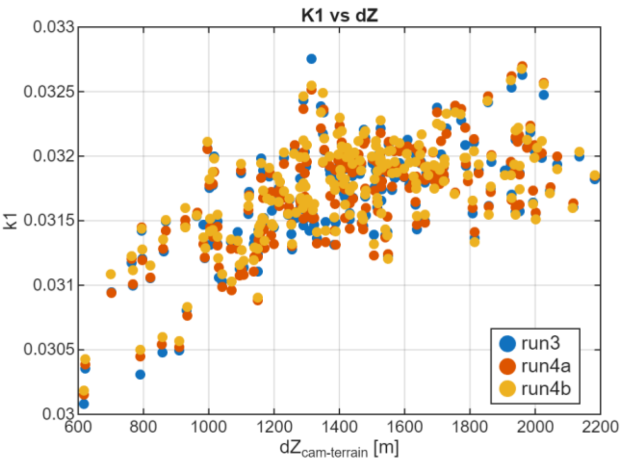

Figure 4. K_1 values as a function of camera-to-terrain distance (dZ) for runs 3, 4a and 4b, showing a consistent positive trend across different control point configurations.

A comparison was performed between the estimated K_1 values and a theoretical proxy derived from the Saastamoinen atmospheric model.
The estimated trend of atmospheric refraction (blue line in Figure 5) shows good agreement with the k_1 values estimated in Metashape, with least-squares residuals two orders of magnitude smaller than the estimated values (Figure 6).

It is therefore possible, starting from images previously corrected for optical distortions, to estimate the atmospheric refraction term K directly from digital photogrammetry software by considering only the parameter k_1 within the calibration process.
In many cases, the estimation of camera calibration parameters does not explicitly separate optical distortion from refractive effects, resulting in parameters with limited physical meaning. The explicit modeling of atmospheric refraction may therefore be particularly important in areas characterized by strong topographic variability, and could support the validation and improvement of experimental models to be applied to photogrammetric flights at high altitudes, such as those typically used for glacier monitoring.

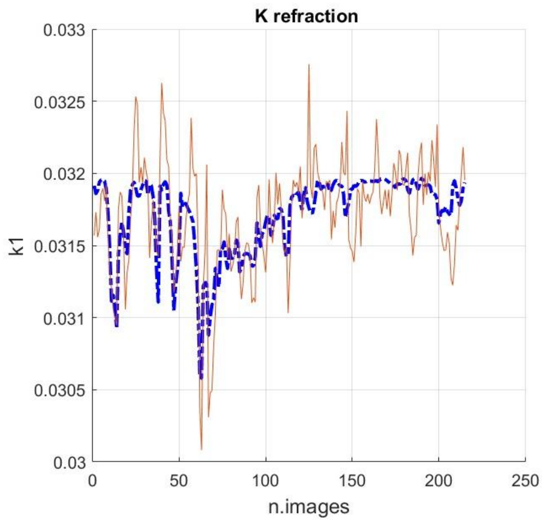

Figure 5. Estimation of the refraction coefficient from the K_1 values of the Brown model. The estimated values are shown in blue, and the experimental K_1 values are shown in red.

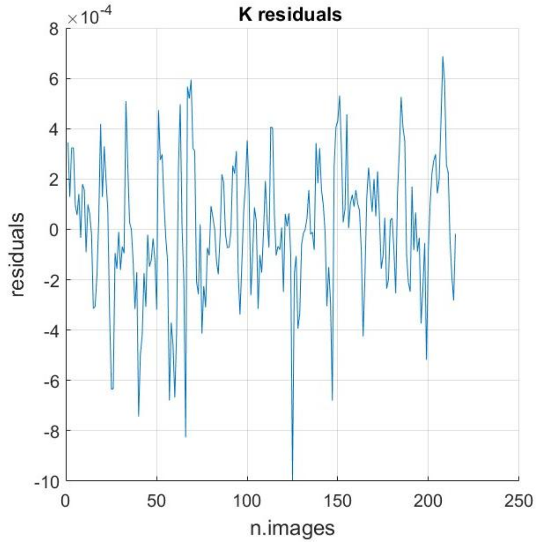

Figure 6. Least squares residuals.

5. Discussion

The radial distortion coefficient k_1 estimated during bundle adjustment cannot be interpreted as a direct measure of atmospheric refraction. Rather, it acts as a compensation parameter that absorbs multiple sources of systematic error, including residual inaccuracies in image undistortion, errors in GCPs, weak block geometry, non-uniform distribution of control points, and inaccuracies in initial camera orientation.
The results obtained in this study show a clear and statistically significant dependence of k_1 on the camera-terrain distance (dZ), which is consistent across different processing configurations and robust to changes in the GCP/check point setup. This suggests that the observed trend reflects a systematic effect related to scene depth rather than random noise or instability in the estimation process.
However, the comparison with the Saastamoinen-based atmospheric proxy reveals only a weak and inconsistent correlation, indicating that the observed variation of k_1 cannot be explained solely by tropospheric refraction. This highlights that

the estimated parameter incorporates a combination of effects, including geometric and numerical components inherent to the photogrammetric model.

In particular, when GCPs are unevenly distributed, such as being concentrated at lower elevations, the risk that k_1 compensates for geometric deformation of the network rather than a physical refractive effect is significant. This behaviour is well documented in photogrammetric literature, where intrinsic parameters are known to partially absorb deficiencies in the external geometry when the network is weakly constrained (Brown, 1971; Fraser, 1997; James and Robson, 2014).

At the same time, the analysis of local geometry indicates that the observed trend is not driven by a reduction in photogrammetric robustness at larger distances, as the number of observed markers increases with dZ. This excludes a simple explanation based on weaker geometric constraints and supports the interpretation of a depth-dependent systematic effect.

Therefore, while the proposed approach is effective as an exploratory tool for detecting systematic behaviours in photogrammetric blocks, the parameter k_1 cannot be considered a direct or independent estimator of atmospheric refraction. Instead, it should be interpreted as a compound parameter reflecting the interaction between acquisition geometry, network configuration, and physical effects.

6. Conclusion

This study investigated the behaviour of the radial distortion parameter k_1 in airborne photogrammetric surveys conducted in a high-relief Alpine environment, with particular focus on its potential relationship with atmospheric refraction.

The results show a clear and statistically significant dependence of k_1 on the vertical camera–terrain distance (dZ), which remains consistent across different bundle adjustment configurations and robust to variations in GCPs distribution. This indicates that the observed effect is not driven by outliers or by local weaknesses in the photogrammetric network, but represents a systematic behaviour of the block related to scene depth.

However, the comparison with a theoretical atmospheric proxy derived from the Saastamoinen model reveals only weak correlation, suggesting that the observed variation of k_1 cannot be attributed solely to atmospheric refraction. Instead, the results indicate that k_1 acts as a compound parameter, absorbing multiple sources of systematic error, including geometric effects, network configuration, and residual modelling inaccuracies.

These findings highlight the limitations of directly interpreting calibration parameters in physical terms, particularly in complex mountainous environments characterized by strong elevation gradients and limited accessibility for control point distribution.

From an operational perspective, the proposed methodology proves effective in detecting depth-dependent systematic effects in photogrammetric blocks and can support the assessment of model reliability in high-altitude surveys. However, a rigorous estimation of atmospheric refraction requires dedicated modelling approaches capable of separating optical, geometric, and atmospheric contributions. Moreover, it should be noted that this work represents a preliminary analysis that requires further investigation. In particular, the strong elevation gradients characterizing the study area introduce additional complexity, making it challenging to disentangle the different contributions absorbed by the estimated parameters, including geometric, radiometric, and atmospheric effects.

Future work should focus on integrating physically-based refraction models within photogrammetric workflows and on improving the distribution and quality of control points, in order to enhance the interpretability and robustness of calibration parameters in challenging environments such as glacierized Alpine areas.

References

Beniston, M., Farinotti, D., Stoffel, M., et al., 2018. The European mountain cryosphere: a review of its current state, trends, and future challenges. The Cryosphere, 12, pp. 759–794.

Brown, D.C., 1971. Close-range camera calibration. Photogrammetric Engineering, 37(8), pp. 855–866.

Fraser, C.S., 1997. Digital camera self-calibration. ISPRS Journal of Photogrammetry and Remote Sensing, 52(4), pp. 149–159. https://doi.org/10.1016/S0924-2716(97)00005-1

Haeberli, W., Schaub, Y., Huggel, C., 2017. Increasing risks related to landslides from degrading permafrost into new lakes in deglaciating mountain ranges. Geomorphology, 293, pp. 405–417.

Hock, R., Rasul, G., Adler, C., et al., 2019. High Mountain Areas. In: IPCC Special Report on the Ocean and Cryosphere in a Changing Climate (SROCC).

Hugonnet, R., McNabb, R., Berthier, E., et al., 2021. Accelerated global glacier mass loss in the early twenty-first century. Nature, 592, pp. 726–731.

Immerzeel, W.W., van Beek, L.P.H., Bierkens, M.F.P., 2010. Climate change will affect the Asian water towers. Science, 328(5984), pp. 1382–1385.

IPCC, 2019. Special Report on the Ocean and Cryosphere in a Changing Climate (SROCC).

IPCC, 2023. Climate Change 2023: Synthesis Report. Contribution of Working Groups I, II and III to the Sixth Assessment Report of the Intergovernmental Panel on Climate Change. IPCC, Geneva, Switzerland.

ISPRA (Istituto Superiore per la Protezione e la Ricerca Ambientale), 2024. Bilancio di massa dei ghiacciai – Regione Valle d’Aosta. Available at: https://climadat.isprambiente.it

Jacquemart, M., Weber, S., Chiarle, M., Chmiel, M., Cicoira, A., Corona, C., Eckert, N., Gaume, J., Giacona, F., Hirschberg, J., Kaitna, R., Magnin, F., Mayer, S., Moos, C., van Herwijnen, A., Stoffel, M., 2024. Detecting the impact of climate change on alpine mass movements in observational records from the European Alps. Earth-Science Reviews, 258, 104886. https://doi.org/10.1016/j.earscirev.2024.104886

James, M.R., Robson, S., 2014. Mitigating systematic error in topographic models derived from UAV and ground-based image networks. Earth Surface Processes and Landforms, 39(10), pp. 1413–1420. https://doi.org/10.1002/esp.3609

La Valpelline, n.d. La Valpelline. Available at: https://www.lavalpelline.it/

Legambiente, 2024. Carovana dei ghiacciai 2024 sui ghiacciai della Valpelline. Available at: https://www.legambiente.it

Remondino, F., Fraser, C., 2006. Digital camera calibration methods: considerations and comparisons. International

Archives of the Photogrammetry, Remote Sensing and Spatial Information Sciences, 36(5), pp. 266–272.

Saastamoinen, J., 1974. Local variation of photogrammetric refraction, Photogrammetric Engineering, 40(3), pp. 295-30

Sottozero VdA, 2025. Ghiacciai 2025. Available at: https://www.sottozerovda.it/ghiacciai-2025/

Stoffel, M., Tiranti, D., Huggel, C., 2014. Climate change impacts on mass movements — Case studies from the European Alps. Science of the Total Environment, 493, pp. 1255–1266.

Viviroli, D., Dürr, H.H., Messerli, B., et al., 2007. Mountains of the world, water towers for humanity. Water Resources Research, 43.

WSL Institute for Snow and Avalanche Research SLF, 2025. Climate change in the Alps: a potential threat. Available at: https://www.slf.ch/en/news/climate-change-in-the-alps-a-potential-threat/

Zemp, M., Huss, M., Thibert, E., et al., 2019. Global glacier mass changes and their contributions to sea-level rise from 1961 to 2016. Nature, 568, pp. 382–386.